ISSUE: January 2020

The Engineer's Guide To EMI In DC-DC Converters (Part 11): Input Filter Impact On Dynamic Performance

by Timothy Hegarty, Texas Instruments, Phoenix, Ariz.

Meeting electromagnetic interference (EMI) standards requires the insertion of an EMI filter between a switching-mode power converter and its source. As described in part 10 of this article series,[1-10] a dynamic coupling between a converter and its EMI filter effectively creates a feedback loop, where the source-side "minor-loop" gain is the ratio of the filter's output impedance (as seen from the converter's input terminals) to the converter's closed-loop input impedance.

When considering the Nyquist plot, the results of small-signal stability analysis are given as a forbidden region that exists outside of a circle with a radius of constant gain margin. The minor-loop gain contour should stay inside this circle for stability to exist. Given the negative input impedance behavior of a regulated, high-loop-gain dc-dc converter, part 10 showed that impedance shaping (via passive damping of the input filter to reduce its output impedance peaking) is normally required to ensure robust stability—the worst-case operating condition being at a minimum input voltage and full load.[10]

Input-filter interactions may severely affect the transfer functions related to dynamic performance of the converter, particularly the loop gain and output impedance characteristics. This part 11 of the series now considers the impact of input-filter interactions on the converter's dynamic performance. Most often, these interactions are caused by resonant circuits within the system. Examples include the output impedance of the EMI filter connected at the converter's input terminals (leading to source-side interactions) and the input impedance of the EMI filter of a downstream converter loading the upstream converter (resulting in load-side interactions).

This discussion begins by presenting a two-port model that can be used to analyze converter dynamics of any dc-dc converter and this model is then used to derive equations that express the system sensitivities to source-side and load-side interactions. These equations are further analyzed to isolate the implicit parameters that influence the converter's dynamic performance. Next, transfer functions are given that express the influence of the source-side (filter output) impedance on converter loop gain and output impedance, as well as the impact of load-side impedance (seen at converter output) on converter loop gain and input impedance.

These expressions are used to explain the relative immunity of a voltage-mode-controlled (VMC) buck converter with input voltage feedforward to source- and load-side interactions. For other cases, equations are given that define what conditions must be met to minimize such interactions. Discussion of the VMC buck converter continues with equations for its open-loop dynamic performance and those needed to design its input EMI filter.

These equations are then used in the next section to analyze a VMC buck converter design example based on the LM5145 controller to observe the impact of input voltage feedforward on the converter's dynamic performance. This performance is also verified with a SIMPLIS simulation.

Analyzing Converter Dynamics

In general, converter transient responses are induced by changes in either the output current or the input voltage, and contain information from the corresponding open-loop transfer function and the loop gain, as you may conclude from Fig. 1. For the output dynamics, $G_{io\text{-}o}(s)$ and $Z_{o\text{-}o}(s)$ denote the internal input-to-output transfer function and the internal output impedance at open loop, respectively. For the input dynamics, $T_{oi\text{-}o}(s)$ and $Y_{in\text{-}o}(s)$ denote the internal reverse-current transfer function and the internal input admittance at open loop, respectively.

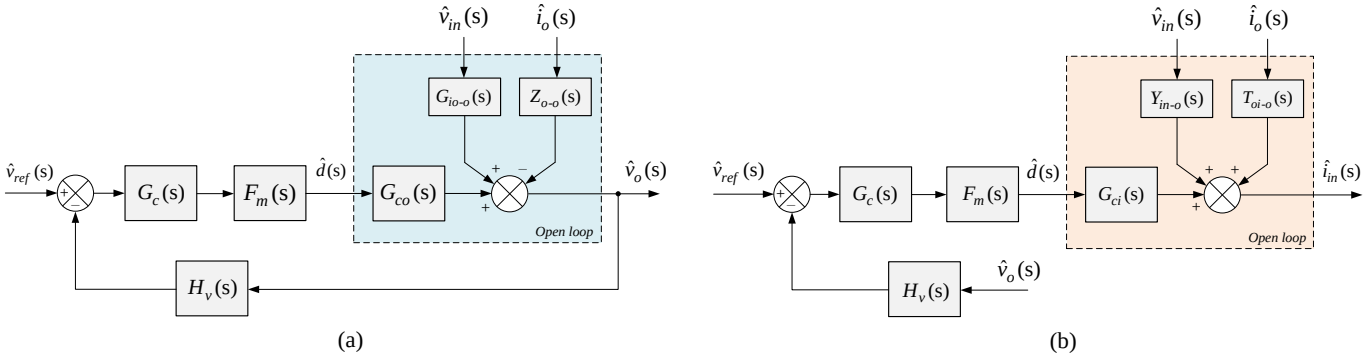

Fig. 1. Control-loop block diagram of open-loop (inside dashed line) and closed-loop converter implementations with output-side feedback: output-side dynamics (a) and input-side dynamics (b).

The corresponding voltage-loop gain from Fig. 1a is $L(s) = H_v(s)G_c(s)F_m(s)G_{co}(s)$, where $H_v(s)$ is the output-voltage sensing gain, $G_c(s)$ is the compensator transfer function, $F_m(s)$ is the modulator gain and $G_{co}(s)$ is the control-to-output voltage transfer function.

There are two primary methods available for analyzing converter dynamics with the addition of an input filter stage:

- Middlebrook's extra element theorem (EET)
- Two-port modeling using G-parameters.

The EET is an analytical tool for linear systems that enables you to assess the influence of an additional impedance element to the original transfer function by employing a correction factor.[11] However, the two-port modeling network structure[12-16] is favored here, as it can represent the internal converter dynamics of any dc-dc converter, independent of topology, control scheme or conduction mode.

The two-port model facilitates consideration of both source- and load-side interactions, and does not require knowledge of the internal converter parameters (information not available with commercial converter modules). Moreover, as you will see, it provides convenient expressions for implicit input-side impedance parameters that are identified and defined in the analysis.

Fig. 2 introduces the two-port G-parameter model with a Norton-equivalent input and Thevenin-equivalent output. Dashed lines denote the internal or unterminated dynamics. A terminated two-port structure then enables the determination of the influence of external source-side and load-side impedances, denoted as $Z_s(s)$ and $Y_L(s)$ in Fig. 2, on the internal transfer function dynamics.

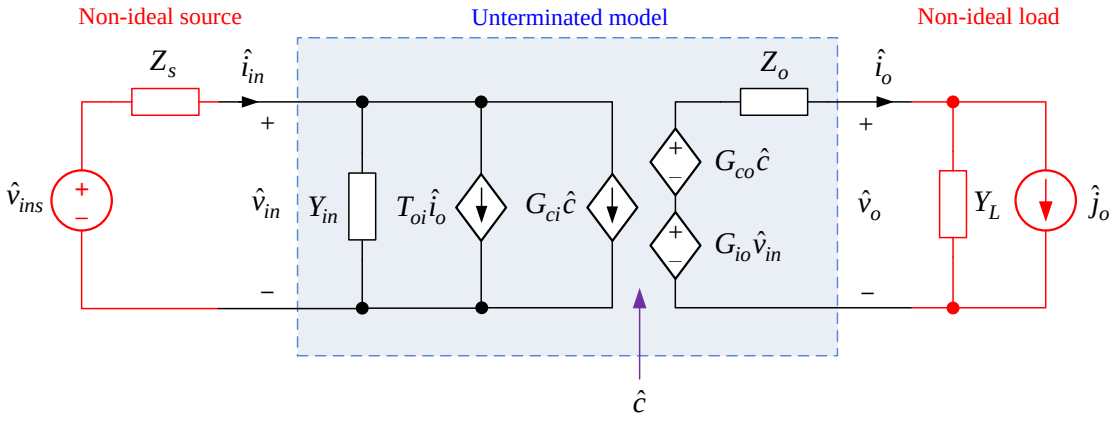

Fig. 2. Linear two-port canonical model of a voltage-fed converter terminated with a nonideal input source (v_{ins}, Z_s) *and nonideal load* (Y_L, j_o)*. The control variable is designated as* c*, while the diamond-shaped symbols denote dependent sources.*

Based on Fig. 2, equation 1 using matrix notation gives the internal or unterminated dynamic representation of a conventional voltage-fed converter using a set of transfer functions being valid both at open loop and closed loop:

$$\begin{bmatrix} \hat{i}_{in}(\mathrm{s}) \\ \hat{v}_o(\mathrm{s}) \end{bmatrix} = \begin{bmatrix} Y_{in}(\mathrm{s}) & T_{oi}(\mathrm{s}) & G_{ci}(\mathrm{s}) \\ G_{io}(\mathrm{s}) & -Z_o(\mathrm{s}) & G_{co}(\mathrm{s}) \end{bmatrix} \begin{bmatrix} \hat{v}_{in}(\mathrm{s}) \\ \hat{i}_o(\mathrm{s}) \\ \hat{c}(\mathrm{s}) \end{bmatrix} \qquad (1)$$

where $v_{in}(\mathrm{s})$ represents an ideal input voltage source with zero source impedance and $i_o(\mathrm{s})$ is an ideal current-source load with infinite output impedance. The hatted notation designates perturbed small-signal variables.

The definition of the transfer functions is obvious when examining the variables in the input vector $\left[\hat{v}_{in}(\mathrm{s}) \quad \hat{i}_o(\mathrm{s}) \quad \hat{c}(\mathrm{s})\right]^{\mathrm{T}}$ and the output vector $\left[\hat{i}_{in}(\mathrm{s}) \quad \hat{v}_o(\mathrm{s})\right]^{\mathrm{T}}$. The variable $\hat{c}(\mathrm{s})$ in the input vector is the general control variable corresponding to $\hat{d}(\mathrm{s})$ for open loop and $\hat{v}_{ref}(\mathrm{s})$ for closed loop, as shown in Fig. 1.

It is possible to assess the influence of finite source impedance on converter dynamics by representing the input voltage using equation 2.

$$\hat{v}_{in}(\mathrm{s}) = \hat{v}_{ins}(\mathrm{s}) - Z_s(\mathrm{s})\hat{i}_{in}(\mathrm{s}) \qquad (2)$$

Substituting this representation into the internal dynamics as expressed by equation 1 yields equation 3,

$$\begin{aligned} \hat{i}_{in} &= Y_{in}\left(\hat{v}_{ins} - Z_s\,\hat{i}_{in}\right) + T_{oi}\,\hat{i}_o + G_{ci}\,\hat{c} \\ \hat{v}_o &= G_{io}\left(\hat{v}_{ins} - Z_s\,\hat{i}_{in}\right) - Z_o\,\hat{i}_o + G_{co}\,\hat{c} \end{aligned} \qquad (3)$$

which then results in the input dynamics of equation 4:

$$\hat{i}_{in} = \frac{Y_{in}}{1+Z_sY_{in}}\hat{v}_{ins} + \frac{T_{oi}}{1+Z_sY_{in}}\hat{i}_o + \frac{G_{ci}}{1+Z_sY_{in}}\hat{c} \qquad (4)$$

and the output dynamics of equation 5, which is further simplified as shown by equation 6:

$$\hat{v}_o = \left(\frac{G_{io} + G_{io}Z_sY_{in} - G_{io}Z_sY_{in}}{1 + Z_sY_{in}} \right) \hat{v}_{ins} - \left(\frac{Z_sG_{io}T_{oi} + Z_o + Z_oZ_sY_{in}}{1 + Z_sY_{in}} \right) \hat{i}_o + \left(\frac{G_{co} - Z_sG_{io}G_{ci} + Z_o + G_{co}Z_sY_{in}}{1 + Z_sY_{in}} \right) \hat{c} \qquad (5)$$

$$\hat{v}_o = \frac{G_{io}}{1 + Z_sY_{in}} \hat{v}_{ins} - \frac{1 + Z_s\left(Y_{in} + \frac{G_{io}T_{oi}}{Z_o} \right)}{1 + Z_sY_{in}} Z_o \hat{i}_o + \frac{1 + Z_s\left(Y_{in} - \frac{G_{io}G_{ci}}{G_{co}} \right)}{1 + Z_sY_{in}} G_{co} \hat{c} \qquad (6)$$

Based on these derivations, equation 7 provides the system dynamics that describe the sensitivity to source-side interactions:

$$\begin{bmatrix} \hat{i}_{in}(\mathrm{s}) \\ \hat{v}_o(\mathrm{s}) \end{bmatrix} = \begin{bmatrix} \frac{Y_{in}}{1 + Z_sY_{in}} & \frac{T_{oi}}{1 + Z_sY_{in}} & \frac{G_{ci}}{1 + Z_sY_{in}} \\ \frac{G_{io}}{1 + Z_sY_{in}} & -\frac{1 + Z_sY_{in\text{-}sc}}{1 + Z_sY_{in}} Z_o & \frac{1 + Z_sY_{in\text{-}\infty}}{1 + Z_sY_{in}} G_{co} \end{bmatrix} \begin{bmatrix} \hat{v}_{ins}(\mathrm{s}) \\ \hat{i}_o(\mathrm{s}) \\ \hat{c}(\mathrm{s}) \end{bmatrix} \qquad (7)$$

Deriving an equivalent set of dynamics (shown in equation 8) enables the modeling of load-side interactions with the load admittance $Y_L(\mathrm{s})$.[12]

$$\begin{bmatrix} \hat{i}_{in}(\mathrm{s}) \\ \hat{v}_o(\mathrm{s}) \end{bmatrix} = \begin{bmatrix} \frac{1 + Z_{o\text{-oci}}Y_L}{1 + Z_oY_L} Y_{in} & \frac{T_{oi}}{1 + Z_oY_L} & \frac{1 + Z_{o\text{-}\infty}Y_L}{1 + Z_oY_L} G_{ci} \\ \frac{G_{io}}{1 + Z_oY_L} & -\frac{Z_o}{1 + Z_oY_L} & \frac{G_{co}}{1 + Z_oY_L} \end{bmatrix} \begin{bmatrix} \hat{v}_{in}(\mathrm{s}) \\ \hat{j}_o(\mathrm{s}) \\ \hat{c}(\mathrm{s}) \end{bmatrix} \qquad (8)$$

The expressions for the implicit input-side parameters that influence $Z_o(\mathrm{s})$ and $G_{co}(\mathrm{s})$ in equation 7—specifically the input admittance with short-circuited output, $Y_{in\text{-}sc}(\mathrm{s})$, and the ideal input admittance, $Y_{in\text{-}\infty}(\mathrm{s})$—are found in equation 6 and expressed by equations 9 and 10:

$$Y_{in\text{-}sc}(\mathrm{s}) = \left. \frac{\hat{i}_{in}(\mathrm{s})}{\hat{v}_{in}(\mathrm{s})} \right|_{\hat{c}=0, \hat{v}_o=0} = Y_{in} + \frac{G_{io}T_{oi}}{Z_o} \qquad (9)$$

$$Y_{in\text{-}\infty}(\mathrm{s}) = \left. \frac{\hat{i}_{in}(\mathrm{s})}{\hat{v}_{in}(\mathrm{s})} \right|_{\hat{v}_o \to 0, \hat{i}_o \to 0} = Y_{in} - \frac{G_{io}G_{ci}}{G_{co}} \qquad (10)$$

$Y_{in\text{-}\infty}(\mathrm{s})$ represents the input admittance measured from the converter input terminals (assuming an ideal feedback controller) and is obtained from the small-signal model by nulling the output voltage.[17] $Y_{in\text{-}\infty}(\mathrm{s})$ is invariant to load, operating mode, control architecture and feedback state (open/closed loop) and is therefore constant for a specific topology, whereas $Y_{in\text{-}sc}(\mathrm{s})$ is only invariant to load and feedback state for a given topology.

The ideal input admittance $Y_{in\text{-}\infty}(\mathrm{s})$ in equation 10 characterizes the closed-loop input admittance of the feedback-controlled converter at low frequencies, where the corresponding feedback loop gain $|L(\mathrm{s})|$ is high, as depicted in equation 11. Therefore, $Y_{in\text{-}\infty}(\mathrm{s})$ is also known as an infinite-bandwidth input admittance. Subscripts *-o* and *-c* denote the open- and closed-loop parameters, respectively.

$$Y_{in\text{-}c}(s) = \frac{1}{1+L(s)} Y_{in\text{-}o}(s) + \frac{L(s)}{1+L(s)} Y_{in\text{-}\infty}(s) \qquad (11)$$

To complete the formulation, the implicit parameters related to the load-side interactions in equation 8 are the ideal output impedance and open-circuit output impedance, defined in equations 12 and 13, respectively:

$$Z_{o\text{-}\infty}(s) = \left.\frac{\hat{v}_o(s)}{\hat{i}_o(s)}\right|_{\hat{i}_{in}=0,\hat{v}_{in}=0} = Z_o + \frac{G_{co}T_{oi}}{G_{ci}} \qquad (12)$$

$$Z_{o\text{-}oci}(s) = \left.\frac{\hat{v}_o(s)}{\hat{i}_o(s)}\right|_{\hat{i}_{in}=0,\hat{c}=0} = Z_o + \frac{G_{io}T_{oi}}{Y_{in}} \qquad (13)$$

A key dynamic feature of these implicit parameters involves the audio-susceptibility (input-to-output) transfer function $G_{io}(s)$, which depends on the applied control scheme. As I will discuss later, $G_{io}(s) \to 0$ results in both source and load invariance, where all input-side admittances are the same and all output-side impedances are the same.

Main Interaction Formulations

Examining the terms in equations 7 and 8, equation set 14 describes the key converter transfer functions:

$$\begin{aligned} L^s(s) &= \frac{1+Z_sY_{in\text{-}\infty}}{1+Z_sY_{in\text{-}o}} L(s) \\ Z_o^s(s) &= \frac{1+Z_sY_{in\text{-}sc}}{1+Z_sY_{in}} Z_o(s) \\ L^L(s) &= \frac{L(s)}{1+Z_{o\text{-}o}Y_L} \\ Y_{in}^L(s) &= \frac{1+Z_{o\text{-}oci}^oY_L}{1+Z_sY_L} Y_{in}(s) \end{aligned} \qquad (14)$$

where the superscripts *S* and *L* designate source- and load-affected transfer functions, respectively. Equation 14 includes the influence of the source-side impedance $Z_s(s)$ on the loop gain $L^s(s)$ and the output dynamics through $Z_o^s(s)$. Also quantified in equation 14 is the effect of the load-side impedance $Y_L(s)$ on the loop gain $L^L(s)$ and input dynamics by $Y_{in}^L(s)$. These expressions are also derivable using the EET;[11, 17-20] however, the implicit source- and load-side impedance parameters are conveniently expressed based on the internal transfer functions when using the two-port model.

In converters where the open-loop audio susceptibility $G_{io\text{-}o}(s) \approx 0$ —such as in a VMC buck converter with input voltage feedforward (VFF) or a peak-current-mode-controlled (PCMC) converter with an appropriate slope compensation ramp amplitude—the source interactions are essentially reduced because $Y_{in\text{-}\infty}(s) = Y_{in\text{-}sc}(s) = Y_{in\text{-}o}(s)$ from equations 9 and 10; thus, the loop gain and output impedance remain unaffected. As a result, $L^s(s) = L(s)$

and $Z_o^S(s) = Z_o(s)$, which makes the converter highly invariant to source-side interactions as well as preventing the load-side interactions from propagating through the converter.

Otherwise, the converter is sensitive to source- and load-related interactions, requiring the conditions in equation 15 for minimal interaction:

$$\begin{aligned} Z_s(s)Y_{in}(s) << 1 \quad &\Rightarrow \quad |Z_s(s)| << \left|Y_{in}(s)^{-1}\right| \\ Z_s(s)Y_{in\text{-}sc}(s) << 1 \quad &\Rightarrow \quad |Z_s(s)| << \left|Y_{in\text{-}sc}(s)^{-1}\right| \\ Z_s(s)Y_{in\text{-}\infty}(s) << 1 \quad &\Rightarrow \quad |Z_s(s)| << \left|Y_{in\text{-}\infty}(s)^{-1}\right| \end{aligned} \qquad (15)$$

Guaranteeing these conditions means that the filter output impedance does not degrade the converter's dynamic performance. Equation 16 provides additional criteria so that the input admittance remains unaltered due to the load impedance interconnection:

$$\begin{aligned} Z_{o\text{-}o}(s)Y_L(s) << 1 \quad &\Rightarrow \quad |Z_{o\text{-}o}(s)| << \left|Y_L(s)^{-1}\right| \\ Z_{o\text{-}oci}(s)Y_L(s) << 1 \quad &\Rightarrow \quad |Z_{o\text{-}oci}(s)| << \left|Y_L(s)^{-1}\right| \end{aligned} \qquad (16)$$

VMC Buck Converter Analysis

Equation 17 gives the open-loop dynamics of a VMC buck converter, with equation 18 defining the equivalent parameters V_E and r_E by including the parasitic resistances of the switches and inductor:[16]

$$\begin{bmatrix} Y_{in\text{-}o}(s) & T_{oi\text{-}o}(s) & G_{ci}(s) \\ G_{io\text{-}o}(s) & -Z_{o\text{-}o}(s) & G_{co}(s) \end{bmatrix} = \frac{\begin{bmatrix} D^2Cs & D(1+sr_CC) & DCV_Es \\ D(1+sr_CC) & -(r_E+sL)(1+sr_CC) & V_E(1+sr_CC) \end{bmatrix}}{s^2LC+s(r_E+r_C)C+1} + \begin{bmatrix} 0 & 0 & I_o \\ 0 & 0 & 0 \end{bmatrix} \qquad (17)$$

$$\begin{aligned} V_E &= V_{in} + (r_{DS2} - r_{DS1})I_o \\ r_E &= D\,r_{DS1} + (1-D)r_{DS2} + r_L \end{aligned} \qquad (18)$$

Table 1 provides the expressions for the input-side impedances that affect input filter design, where $|R_L|$ represents the ohmic property of the load impedance, which can be a conventional load resistance or the negative incremental input resistance of a downstream converter. I would encourage you to review references [12] to [19] for expressions applicable to VMC and other commonly used control schemes. The use of these equations will be demonstrated in the design example presented in the next section.

Table 1. Input filter design impedances for a VMC buck converter.

Input impedance	Circuit element expression
Unterminated open-loop Z_{in} $Z_{in\text{-}o}(s) = Z_{in}(s)\big\|_{\hat{d}(s)=0}$	$Z_{in\text{-}o}(s) = \frac{s^2 LC + s(r_E + r_C)C + 1}{sD^2 C}$
Load-affected open-loop Z_{in} $Z^L_{in\text{-}o}(s) = Z^L_{in}(s)\big\|_{\hat{d}(s)=0}$	$Z^L_{in\text{-}o}(s) = \frac{\lvert R_L\rvert}{D^2} \frac{s^2 LC + s\left[(r_E + r_C)C + \frac{L}{\lvert R_L\rvert}\right] + 1}{1 + s\lvert R_L\rvert C}$
Closed-loop Z_{in} $Z_{in\text{-}c}(s) = Z_{in}(s)\big\|_{\hat{i}_o(s)=0}$	$Z_{in\text{-}c}(s) = \frac{[1 + L(s)]Z^L_{in\text{-}o}(s)}{1 - [D^2/R]L(s)Z^L_{in\text{-}o}(s)}$
Closed-loop Z_{in} with output voltage nullified ("ideal" Z_{in}) $Z_{in\text{-}\infty}(s) = Z_{in}(s)\big\|_{\hat{v}_o(s)\to 0}$	$Z_{in\text{-}\infty}(s) = -\frac{V_E}{DI_o} \approx -\frac{V_{in}}{I_{in}}$
Open-loop Z_{in} with output port shorted $Z_{in\text{-}sc}(s) = Z_{in}(s)\big\|_{\hat{c}(s)=0, \hat{v}_o(s)=0}$	$Z_{in\text{-}sc}(s) = \frac{r_E + sL}{D^2}$

Assessing Dynamic Performance Via Analysis And Simulation

Fig. 3 shows the SIMPLIS schematic of a synchronous buck dc-dc regulator using parameters applicable to the Texas Instruments LM5145 voltage-mode controller[21] with input voltage feedforward. The steady-state input voltage range is 18 V to 36 V with transient excursions to 60 V, aligning with typical supplies used in industrial applications, and the switching frequency is 500 kHz. The regulated output is 5 V at a maximum load current of 25 A. Component selection for the type-3 compensation network sets the voltage-loop crossover frequency at 40 kHz with greater than 60 degrees of phase margin (before adding the input filter).

A single-stage filter with a resonant frequency close to 20 kHz connects at the input to provide differential-mode noise attenuation. An RL parallel-damped circuit connects across the input filter inductor, Lf. The damping inductance is set at half the filter inductance, and the damping resistance is equal to the filter characteristic impedance. Between the EMI filter and the buck power stage is a perturbation source (also described in part 10) to facilitate the measurement of impedance and audio susceptibility.

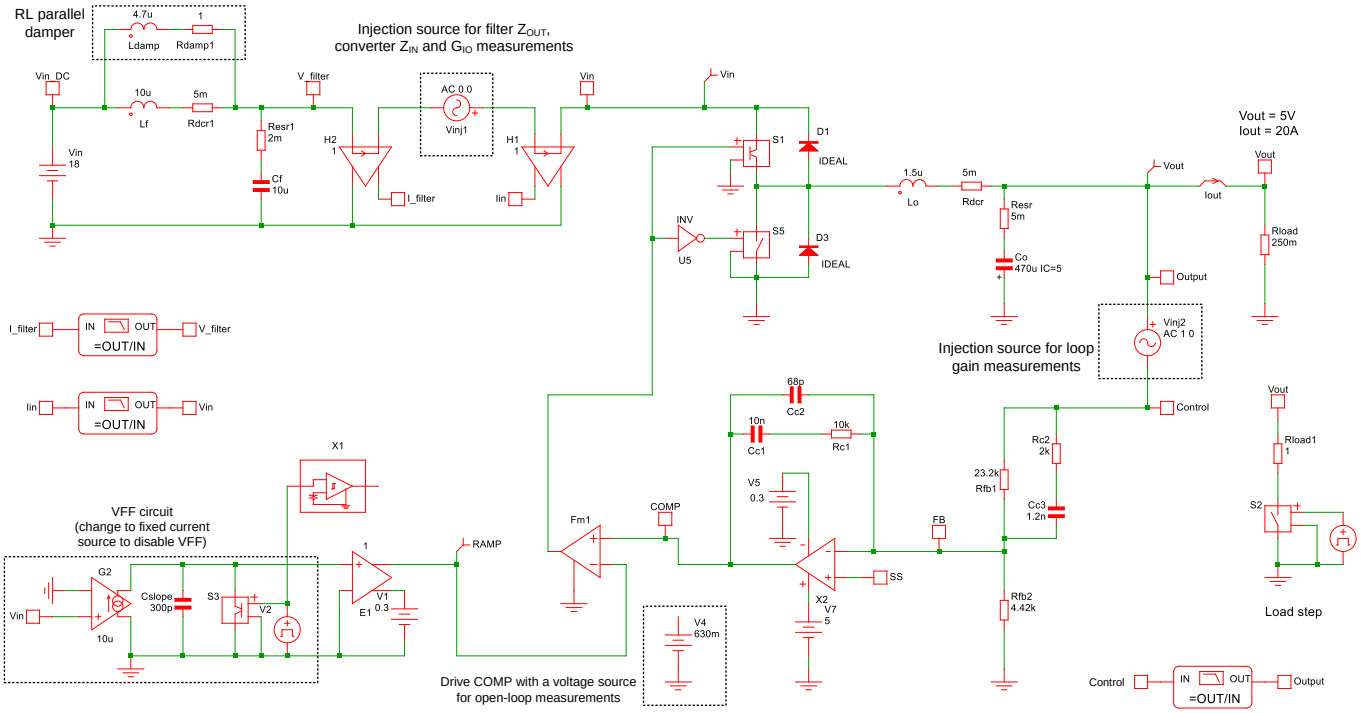

Fig. 3. SIMPLIS simulation schematic of a voltage-mode-controlled synchronous buck regulator with an RL parallel-damped input filter. V_{IN} = 18 V, V_{OUT} = 5 V and I_{OUT} = 20 A.

Fig. 4 shows the calculated impedance characteristics of the filter and converter in Fig. 3 using the expressions from Table 1 for a voltage-mode converter. While $Z_{in\text{-}sc}(s)$ is the lowest impedance at low frequency, note that $Z_{in\text{-}o}(s)$ at the converter's resonant frequency of 6 kHz overlaps with the EMI filter output impedance $Z_s(s)$, pointing to a source interaction of the loop gain according to equation 14.

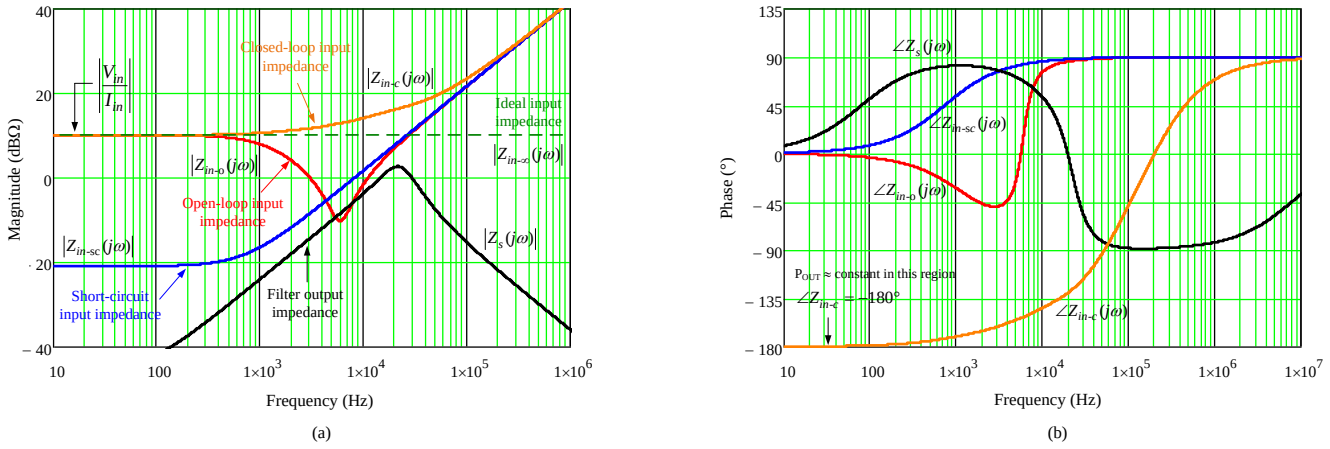

Fig. 4. Checking for overlap of EMI filter output impedance magnitude (a) with converter open-loop/short-circuit/ideal input impedances. The phase (b) provides further insight.

Fig. 5a presents the simulation results of the loop gain with and without the input filter connected. The plots indicate distinct gain and phase disturbances. Distortion is also evident in the time-domain load transient response in Fig. 5b.

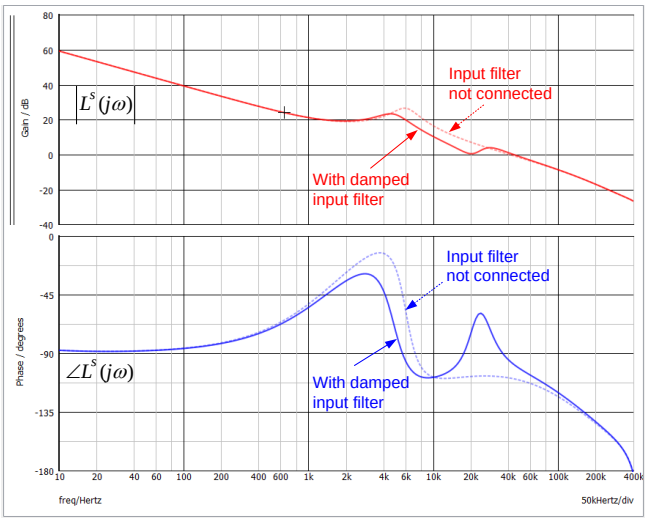

(a)

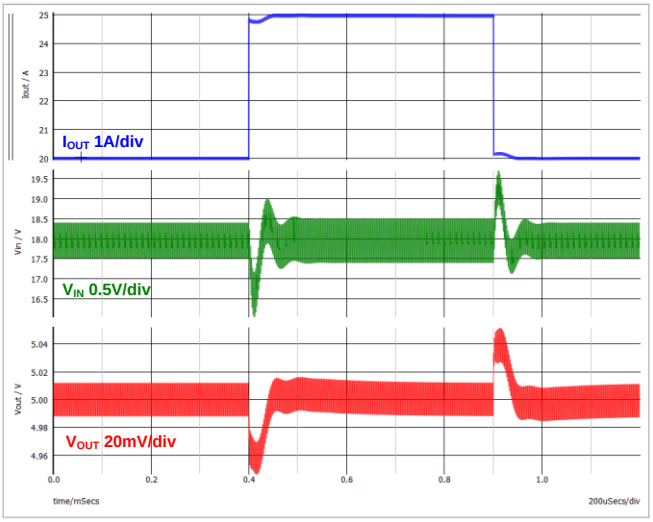

(b)

Fig. 5. Evidence of distortion related to source-side interactions (VFF disabled): Bode plot of loop gain (a); and load transient response (b) of the voltage-mode converter.

Fig. 6 shows the loop gain and transient response when VFF is enabled. Clearly, the frequency domain and time domain behaviors are much more robust. In addition to input-noise attenuation performance (comparable to that achieved by peak-current-mode control) and voltage-loop gain independent of the input voltage, VFF provides much-reduced input filter interactions compared to conventional voltage-mode control.

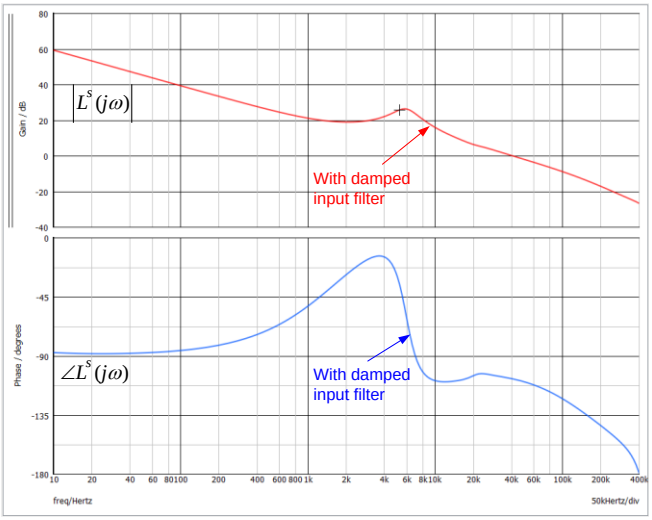

(a)

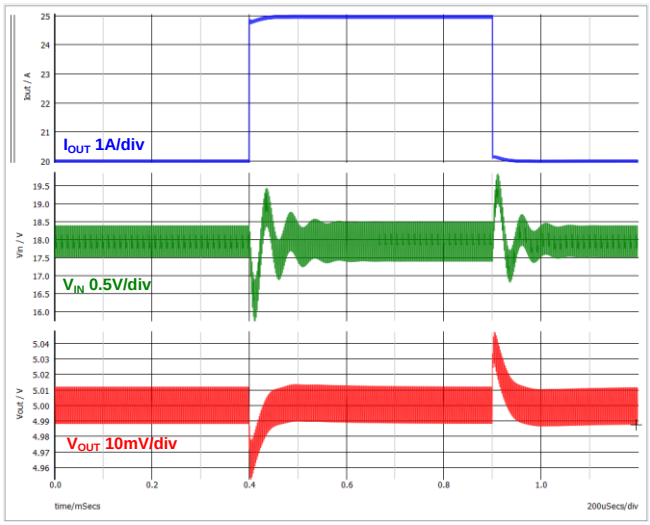

(b)

Fig. 6. Mitigation of source-side interactions by enabling VFF: Bode plot of voltage loop gain (a); and load transient response (b).

Fig. 7 shows plots of open-loop audio susceptibility $G_{io\text{-}o}(s)$ and open-loop input impedance $Z_{in\text{-}o}(s)$, both with and without VFF.[16] An approximate 40-dB improvement in the input rejection characteristic up to the loop crossover frequency is evident with VFF enabled. Given equations 9 and 10, this improvement indicates that the converter with feedforward has reduced interaction sensitivity and is more invariant to source-side interactions.

Note also that the open-loop input impedance in Fig. 7b with VFF enabled has a low-frequency phase of -180 degrees, similar to the constant-power load characteristic discussed in part 10. Theoretically, an open-loop converter with VFF—such as an unregulated intermediate bus converter commonly found in distributed power architectures—can become unstable when an input filter is connected.[16]

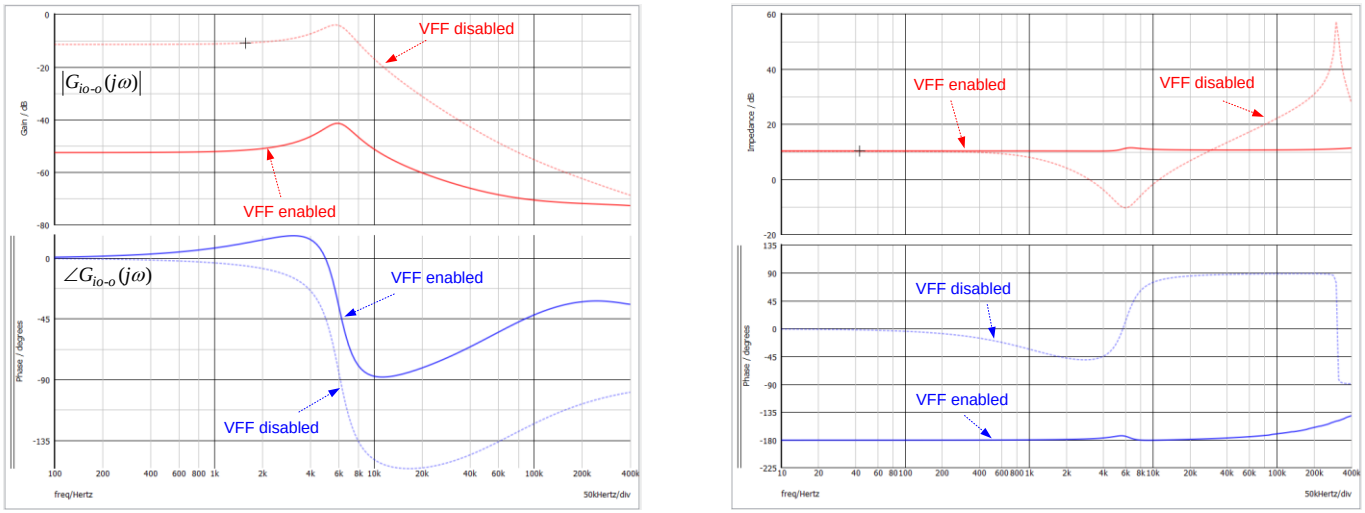

(a) (b)

Fig. 7. Plot of open-loop audio susceptibility (a) and open-loop input impedance (b).

Summary

The combination of a switched-mode converter and an EMI filter forms a dynamically demanding system that is prone to instability and transient performance degradation. Of particular concern is the resonant behavior of the filter output impedance, where overlap with the converter's input impedances (in both explicit and implicit forms) can occur over a certain frequency range. Impedance shaping via damping provides stability while preserving the converter's dynamic performance.

In addition to the implicit admittance and impedance parameters, key elements of the dynamic profile are:

- the control-to-output transfer function $G_{co}(s)$ that contributes to the output-voltage loop gain $L(s)$;
- the open-loop output impedance $Z_{o\text{-}o}(s)$ mainly determining the load interactions;
- the open-loop input admittance $Y_{in\text{-}o}(s)$ mainly affecting the source interactions;
- and the audio susceptibility transfer function $G_{io}(s)$ determining the level of source invariance that a converter may exhibit.

Clearly, input filter design requires prior knowledge and careful consideration of converter dynamics.

References

1. "The Engineer's Guide To EMI In DC-DC Converters (Part 1): Standards Requirements And Measurement Techniques" by Timothy Hegarty, How2Power Today, December 2017 issue.
2. "The Engineer's Guide To EMI In DC-DC Converters (Part 2): Noise Propagation and Filtering" by Timothy Hegarty, How2Power Today, January 2018 issue.

3. "The Engineer's Guide To EMI In DC-DC Converters (Part 3): Understanding Power Stage Parasitics" by Timothy Hegarty, How2Power Today, March 2018 issue.
4. "The Engineer's Guide To EMI In DC-DC Converters (Part 4): Radiated Emissions" by Timothy Hegarty, How2Power Today, April 2018 issue.
5. "The Engineer's Guide To EMI In DC-DC Converters (Part 5): Mitigation Techniques Using Integrated FET Designs" by Timothy Hegarty, How2Power Today, June 2018 issue.
6. "The Engineer's Guide To EMI In DC-DC Converters (Part 6): Mitigation Techniques Using Discrete FET Designs" by Timothy Hegarty, How2Power Today, September 2018 issue.
7. "The Engineer's Guide To EMI In DC-DC Converters (Part 7): Common-Mode Noise Of A Flyback" by Timothy Hegarty, How2Power Today, December 2018 issue.
8. "The Engineer's Guide To EMI In DC-DC Converters (Part 8): Mitigation Techniques For Isolated Designs" by Timothy Hegarty, How2Power Today, February 2019 issue.
9. "The Engineer's Guide To EMI In DC-DC Converters (Part 9): Spread-Spectrum Modulation" by Timothy Hegarty, How2Power Today, August 2019 issue.
10. "The Engineer's Guide To EMI In DC-DC Converters (Part 10): Input Filter Impact On Stability" by Timothy Hegarty, How2Power Today, November 2019 issue.
11. "Null double injection and the extra element theorem" by R.D. Middlebrook, *IEEE Transactions on Education* 32, No. 3 (August 1989), pp. 167-180.
12. "Analysing the dynamics of regulated converters" by Teuvo Suntio et al, *IEE Proceedings – Electric Power Applications* 153, No. 6 (November 2006), pp. 905-910.
13. "Dynamic profile of switched-mode converters: modeling, analysis and control" by Teuvo Suntio, Wiley-VCH, April 2009.
14. "Methodology for dynamic stability and robustness analysis of commercial-power-module-based DC-distributed systems" by Sanna Vesti, Ph.D. thesis, Tampere University of Technology, 2015.
15. "Effect of control method on impedance-based interactions in a buck converter" by Sanna Vesti et al, *IEEE Transactions on Power Electronics* 28, No. 11 (Nov. 2013), pp. 5311-5322.
16. "Dynamical characterization of input-voltage-feedforward-controlled buck converter" by Matti Karppanen et al, *IEEE Transactions on Industrial Electronics* 54, No. 2 (April 2007), pp. 1005-1013.
17. "Fundamentals of Power Electronics" by Robert Erickson and Dragan Maksimovic, Springer, second edition, 2001.
18. "Input impedance analysis of PWM DC-to-DC converters" by Dingsoo Kim et al, Applied Power Electronics Conference 2006, pp. 1339-1346.
19. "Analysis of input filter interactions in switching power converters" by Byungcho Choi et al, *IEEE Transactions on Power Electronics* 22, No. 2, (March 2007), pp. 452-460.
20. "Closed-loop input and output impedances of DC-DC switching converters operating in voltage and current mode control" by Reza Ahmadi et al, IEEE Industrial Electronics Society Annual Conference, November 2010, pp. 2311-2316.
21. LM5145 wide input voltage (V_{IN}) range synchronous buck controller high density evaluation module.

About The Author

Timothy Hegarty is an applications engineer for the Buck Switching Regulators business unit at Texas Instruments. With over 22 years of power management engineering experience, he has written numerous conference papers, articles, seminars, white papers, application notes and blogs.

Tim's current focus is on enabling technologies for high-frequency, low-EMI, isolated and nonisolated regulators with wide input voltage range, targeting industrial, communications and automotive applications in particular. He is a

senior member of the IEEE and a member of the IEEE Power Electronics, Industrial Applications and EMC Societies.

For more information on EMI, see How2Power's Power Supply EMI Anthology. Also see the How2Power's Design Guide, locate the Design Area category and select "EMI and EMC".